NOTE

Reducing crosstalk in optically-pumped magnetometer arrays

IOP Publishing Phys. Med. Biol. 64 (2019) 21NT03 (7pp) https://doi.org/10.1088/1361-6560/ab4c06

Physics in Medicine & Biology

IPEM Institute of Physics and Engineering in Medicine

NOTE

Reducing crosstalk in optically-pumped magnetometer arrays

N V Nardelli[1], S P Krzyzewski[1] and S A Knappe[1,2,3]

[1] University of Colorado Boulder, Boulder, CO 80309, United States of America
[2] FieldLine Inc., Boulder, CO 80301, United States of America
[3] Author to whom any correspondence should be addressed.

E-mail: svenja.knappe@colorado.edu

Keywords: magnetometer, atomic, laser sensors, optical instruments, micro-optical devices, MEG, OPM

RECEIVED
25 July 2019

REVISED
3 October 2019

ACCEPTED FOR PUBLICATION
8 October 2019

PUBLISHED
4 November 2019

Abstract

Optically pumped magnetometers (OPMs) operating in the spin-exchange relaxation-free regime are emerging as alternative sensors to superconducting quantum interference devices (SQUIDs) for magnetoencephalography (MEG). As the number of OPMs in a single imaging system increases to rival SQUID MEG systems, cross-talk between nearby sensors limits the measurement accuracy. We experimentally demonstrate a coil geometry, which generates an order of magnitude less cross-talk (less than 0.5%) than a Helmholtz coil (8%). The new coil design is simple and compact, requiring two coaxial coil pairs that add 1 mm to the 6 mm radius and is driven by a single current driver. The new design maintains a magnetic field homogeneity over the volume of the magnetometer of more than 94%, which is sufficient for the zero-field OPM to operate in a 200 nT ambient field environment. Our result increases the feasibility of high-spatial resolution OPM-based bio-magnetic imaging technology due to the reduction of cross-talk at high sensor density.

1. Introduction

Magnetoencephalography (MEG) measures small magnetic fields (femtotesla to picotesla) generated by neuronal currents within the brain and has led to insights into neural activity at millisecond time scales (Supek and Aine 2014). Most MEG systems are based on low-temperature superconducting quantum interference devices (SQUIDs). The SQUIDs are housed in a helmet-shaped liquid helium dewar with roughly 2 cm of space between the SQUIDs and the inside surface of the helmet. Since the magnetic field falls off quickly with distance from the source, e.g. $1/r^3$ for magnetic dipoles, the distance between the sensors and scalp is important for the quality of the MEG images. This problem is compounded by the fixed positions of the low-temperature SQUIDs cannot account for differences in a patient's head shape and size. On-scalp sensors, such as optically-pumped magnetometers (OPMs) and arrays of high-temperature SQUIDs (Zhang *et al* 1993, Dammers *et al* 2014, Pfeiffer *et al* 2019), can be arranged in geometries conformal to the head, independent of the size and shape. Recent studies simulating whole-head MEG systems with on-scalp sensors promise greatly increased spatial resolution compared to the current SQUID-based MEG systems (Luessi *et al* 2014, Boto *et al* 2016, Iivanainen *et al* 2017).

In the OPMs used here, ^{87}Rb atoms are confined in a microfabricated vapor cell (Liew *et al* 2004) made from silicon and glass. Light at 795 nm, on resonance with the D1 transition in ^{87}Rb, is circularly polarized and used to create a spin-polarization in the ^{87}Rb atoms. The transmitted light power is altered as a function of the magnetic field at the location of the vapor cell. A detailed description of the sensor geometry can be found in Sheng *et al* (2017). In order to reach high field sensitivities, the OPMs are operated in the regime where decoherence from spin-exchange collisions is suppressed: at very low ambient magnetic fields and high ^{87}Rb densities (Happer and Tang 1973, Allred *et al* 2002). Nitrogen at a density of roughly 1 amagat is used as a buffer gas to inhibit ^{87}Rb collisions with the cell walls as well as a quenching gas to limit radiation trapping, both of which are necessary to increase the spin-coherence time at high density. The zero-field resonance is measured by monitoring the transmission of light from a single laser beam through the vapor cell (Dupont-Roc *et al* 1969). This creates a symmetric resonance lineshape centered around zero magnetic field. A small magnetic modulation field of a few kilohertz and about 100 nanotesla is applied in a direction perpendicular to the laser beam. Phase-sensitive detection of the transmission signal at this modulation frequency yields a dispersive resonance as the magnetic

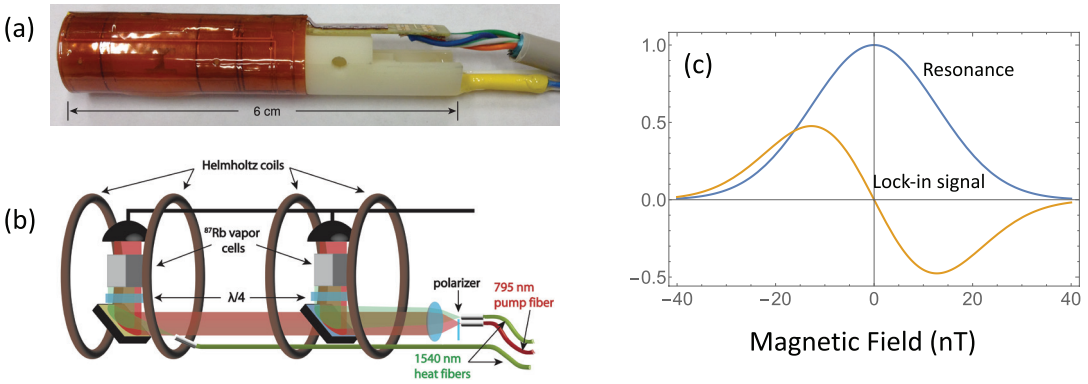

Figure 1. (a) Photograph of an optically-pumped gradiometer and (b) schematic of the gradiometer interior. 1540 nm light used to heat the vapor cells is shown in green and 795 nm light used for probing ^{87}Rb atoms is shown in red. (c) Photodiode signal (blue) and lock-in signal (orange) when the DC field along the cylinder axis of the magnetometer is scanned around zero.

DC field in the direction of the modulation field is scanned. For increased sensor linearity and dynamic range, the OPM is operated under negative feedback by locking the DC field to the zero-crossing of this resonance. The output of the magnetometer is then given by the current applied to the coils in order to keep the magnetometer in a zero-field environment. The modulation field is generated by a Helmholtz coil pair of radius 6.1 mm. It is patterned onto a flexible Kapton circuit board, which is wrapped around the cylindrical sensor housing shown in figure 1(a). The same Helmholtz coil can apply the negative feedback field to keep the sensor locked to the zero-field crossing resonance. In the current sensors, two parallel magnetometers are integrated in the same cylindrical sensor head: one cell is centered 4 mm from the tip of the sensor and the second 2 cm away. This allows for measurements of a magnetic field gradient in addition to the field itself.

MEG systems require a dense array of magnetometers for localization of magnetic sources in the brain with good spatial resolution. As OPM density increases, the modulation and negative feedback fields are sensed by neighboring sensors. When OPMs are operated in an open-loop configuration (no feedback), a neighboring OPM can add fields that influence the effective sensor orientation, i.e. the axis of the directional magnetometer. Unless two magnetometers are very close and are oriented at an angle that is large, this effect is small (a maximum of 5°) (Boto *et al* 2018). When OPMs operate in a closed-loop configuration, however, the field information of one sensor is imprinted onto its feedback coil and can be seen by neighboring sensors.

For two identical cylindrical Helmholtz coil pairs oriented parallel to one another (touching on a tangent and aligned with their axis of symmetry) about 8% of the field amplitude at the center of one coil is present at the center of the other. To reduce cross-talk in a dense OPM array it is necessary to employ a coil configuration that generates much less field outside of the coil volume than a Helmholtz coil. SQUID MEG systems, which support hundreds of magnetometers arrayed around the head, also contend with cross-talk, which arises from the mutual inductance of adjacent sensors. These systems mitigate this issue through software (Taulu 2008) or hardware (ter Brake *et al* 1986, Schwarz *et al* 2015) methods and have achieved cross-talk levels as low as 0.5% (Ruffieux *et al* 2017).

For zero-field OPMs, all-optical methods that do not require physical coils have also been investigated. One technique modulates the intensity or frequency of the pump light to create a dispersive resonance (Jiménez-Martínez *et al* 2014). These methods have no cross-talk but require large light powers and achieve sensitivities of only a few pT/Hz$^{1/2}$.

We have designed and demonstrated a coil geometry which reduces cross-talk of adjacent coils to less than 0.5% of the field at coil center. The new coil geometry preserves the appealing properties of a Helmholtz coil, including field uniformity across the microfabricated vapor cell as well as simplicity and compactness.

2. Simple gradiometer design

Our current OPM system for MEG consists of an array of 22 gradiometers operating under negative feedback, each containing two magnetometers separated by 2 cm (Perry *et al* 2017). They are placed on the scalp such that the sensitive direction is pointing normal to the head surface. Each of the two magnetometers is controlled independently by a circular Helmholtz coil pair.

To assess the crosstalk between neighboring sensors, a current was applied to the coils on one sensor and modulated sinusoidally at 10 Hz. A second sensor was placed with its cylindrical axis parallel to the first (worst-case scenario). The radial distance of the two sensors was varied and the amplitude of the 10 Hz modulation was measured by the neighboring sensor. Figure 2(c) shows the measured cross-talk as a function of radial

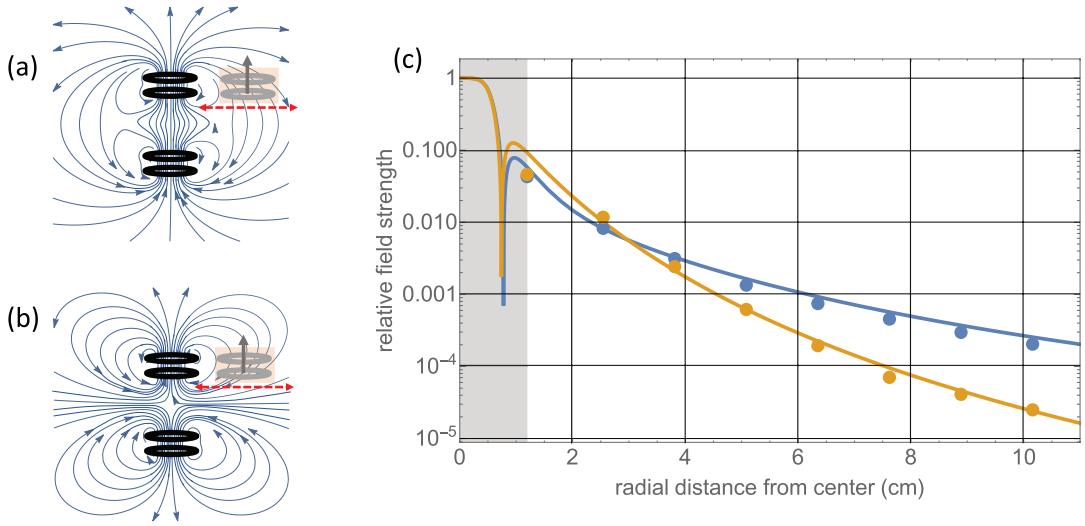

Figure 2. (a) Magnetic field pattern of sensors with Helmholtz pairs driven in-phase and (b) driven 180° out-of-phase. (c) Magnetometer, shown in (a) and (b) in orange, measures the axial field as a function of radial distance. The blue points represent the measured field when Helmholtz pairs are driven in-phase and the orange points represent the measured field when the coils are driven out-of-phase. The blue and orange traces represent the theoretical field predictions for each case. The gray region indicate space occupied by the sensor body.

center-to-center distance between two gradiometers when both Helmholtz coils on the gradiometer were active. The magnetic field strength is normalized to the field at the center of the magnetometer. Cross-talk was measured experimentally (points in figure 2(c)) and compared to the calculations of the expected field (solid lines) (Simpson *et al* 2001). To predict the field, we add the magnetic fields created by several current loops along the loop axis (z),

$$B_{z,loop} = \frac{C}{2\alpha^2\beta}\left[\left(a^2-\rho^2-z^2\right)E\left(k^2\right)+\alpha^2 K\left(k^2\right)\right], \tag{1}$$

where $C=\mu_0 I/\pi, \alpha^2=a^2+\rho^2+z^2-2a\rho, \beta^2=a^2+\rho^2+z^2+2a\rho, k^2=1-(\alpha/\beta)^2$ and E and K represent elliptic integrals of the first and second kind. z is the axial coordinate, ρ is the radial coordinate and a is the loop radius. We compare the cases when the two Helmholtz coil pairs on the gradiometer were driven in phase (figure 2(a)) and driven 180° out of phase (figure 2(b)).

We find that modulating the two Helmholtz coil pairs 180° out of phase reduces the cross-talk between sensors if they are at least 3 cm apart. In this limit, the in-phase coils create a dipole field whereas the out-of-phase coils create a quadrupole field. This is helpful in our current MEG array where the sensor spacing is sufficiently large. However, in more compact designs, a new coil design is required.

3. Reduced cross-talk design

Helmholtz coils are desirable for microfabricated magnetometers because of the high field uniformity at the coil center while remaining compact. Uniformity is especially important over the volume of the vapor cell since it influences the dynamic range of the zero-field OPM. It is therefore necessary to design a coil that maintains field uniformity around the center while generating very little field outside of the coil geometry. In addition, the design needs to preserve simplicity and compactness.

A secondary coil pair was added with a 7 mm radius to partially cancel the field of the inner 6 mm radius Helmholtz coil (figure 3(c)). Currents in the two coil pairs are applied in opposite directions to create opposing fields with an inner/outer current ratio of 3:2 which is achieved by 3 inner turns and 2 outer turns. The ends of the wire from each coil were tightly twisted to minimize excess fields produced by unwanted sources. On a flexible printed circuit, this can be achieved by locating the incoming and outgoing leads directly on top of one another.

The 6 mm and 7 mm radii and 3/2 turn ratio were chosen jointly to simultaneously maximize the field fall-off outside of the geometry and maximize the field homogeneity across the central volume using the theoretical coil model in equation (1). The integer number of coil turns allows for operation with a single current driver instead of two drivers with independently controlled current amplitude and phase. Since we used a rigid tube to wrap the inner coils, the outer radius was the free parameter of which we had most control. An outer radius of 7 mm was found to satisfy our field requirements.

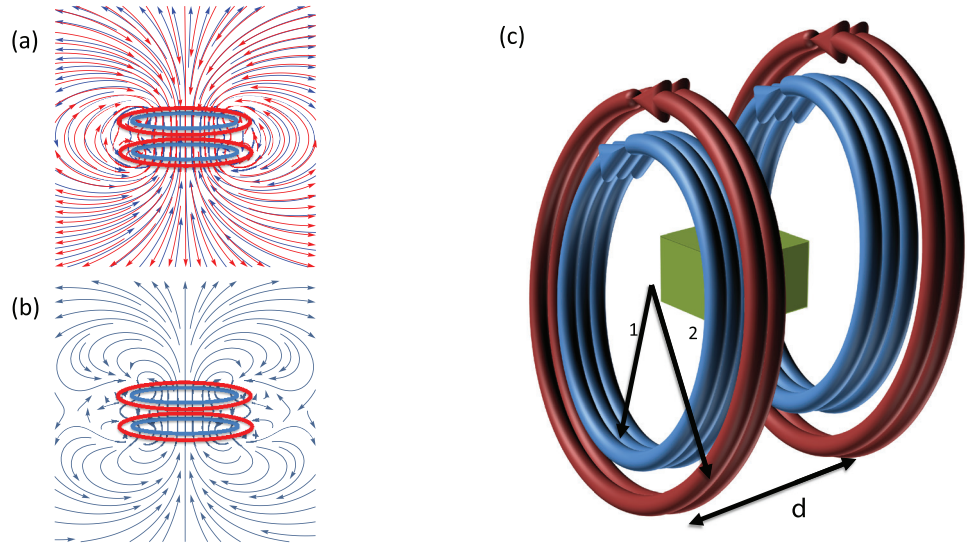

Figure 3. New coil geometry for reduced cross-talk. (a): field lines for each coil are shown in blue and red and (b): field lines for the combined coils. (c): the blue coils are Helmholtz with a radius of $R_1 = 6$ mm and are spaced by $d = 6$ mm. The red coils are aligned with the blue coils but have opposite current and a radius of $R_2 \sim 7$ mm. The green box in the center represents the microfabricated vapor cell.

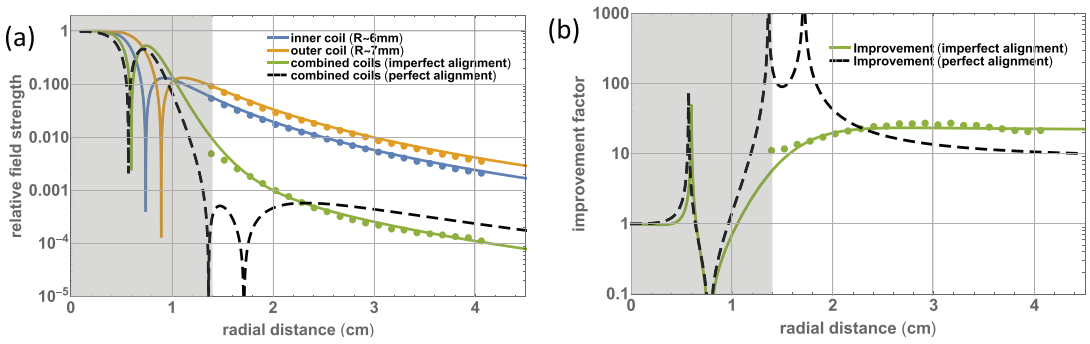

Figure 4. (a) Measurements of axial field fall-off as a function of radial position. The blue, orange and green points represent inner and outer coils, respectively, driven separately and then driven together. The solid lines indicate the theoretical predictions. The dashed black line shows the theoretical field of the combined coils if aligned perfectly. (b) The improvement in field fall-off of the new coil set versus the old Helmholtz coil (the blue points and curve) and the dashed black line represents the improvement potential if coils are aligned perfectly. The gray regions indicate space occupied by the sensor body. The singularities in both plots are an artifact of the log scaling since the field values cross zero and become negative.

When calculating the combined magnetic field from the two coil pairs the field outside of the sensor is reduced by a factor of 100 (black dashed line in figure 4(b)) within 1.8 cm of the center of the sensor, where unwanted magnetic fields tend to be largest. Two adjacent sensors with this new coil geometry will have a minimum radial distance (center-to-center) of 14 mm and the sensing volume, defined by the microfabricated alkali vapor cell (green cube in figure 3), occupies at most 3 mm at coil center.

A gradiometer consisting of two coils, as in section 2, would show similar field fall-off when the coil sets are driven in and out of phase. Analysis using equation (1) shows that cross-talk is limited to 0.1% for nearest neighbors with both in-phase and out-of-phase fields. For secondary neighbors this falls to 0.06% for in-phase fields and 0.03% for out-of-phase fields.

3.1. Experimental demonstration

Inner and outer coils were wrapped with 28-gauge wire and separated by 18 wraps of Kapton tape (0.05 mm thickness). The new coil assembly was mounted on a micrometer stage and a zero-field OPM measured the axial field strength (the component parallel to the coil axis) at different radial positions. A 10 Hz sinusoidal current of 200 μA was applied to the inner only, outer only, or both coils at once to produce the three sets of points in figure 4(a). Measurements were performed in a four-layer mu-metal shield.

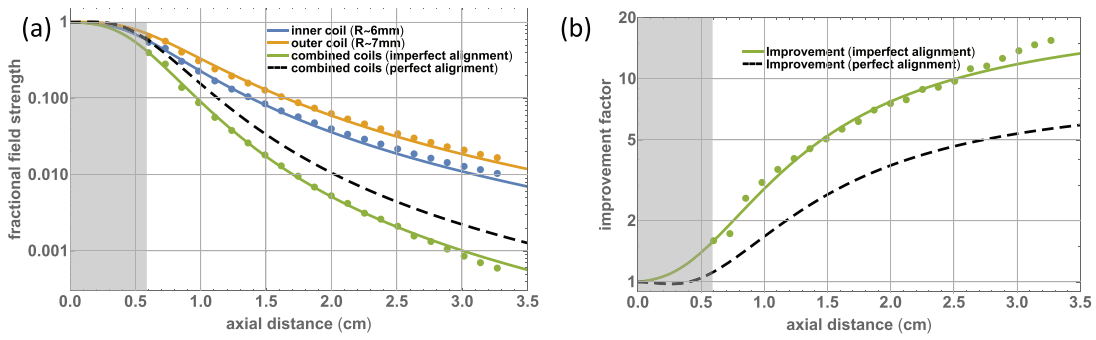

Figure 5. (a) Axial field fall-off as a function of axial distance. Blue, orange and green points represent inner, outer and combined fields, respectively and the corresponding solid curves represent their theoretical predictions. The dashed black curve represents the field of the combined coils if perfect alignment is assumed. (b) Improvement of new coil geometry in the axial direction. Blue points and curve are the improvement of the new geometry over a simple Helmholtz and the black dashed curve is the expected improvement assuming perfect coil alignment. The gray regions indicate space occupied by the sensor body.

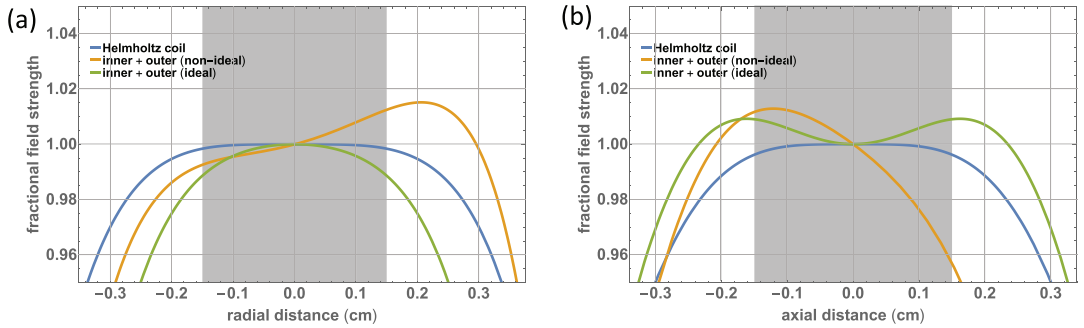

Figure 6. Field homogeneity of the axial field about the coil center along the radial direction (a) and the axial direction (b). The blue curves represent the original Helmholtz coil, the orange curves represent the new coil set with errors included and the green curves represent the new coil set with perfect alignment. The shaded regions represent the volume occupied by the 3 mm vapor cell.

In figure 4, the experimental data for the inner and outer coil's field matched the calculations well (orange and blue points/curves). In contrast, the measured field does not match the theory when both coil sets are operated together (green points and black dashed curve). By adjusting the model parameters such as coil diameter and axial deviation within a few tenths of a millimeter (inner/outer coil radial separation: −0.14 mm, inner coil pair axial separation: −0.22 mm, outer coil pair axial separation: +0.13 mm, coil pair axial separation: +0.14 mm, outer coil radius skew: 0.5 mm, inner coil angle skew: −1.67°, outer coil angle skew: −0.12°), we adjust the theoretical prediction to best match the experimental data. These variations fall within the uncertainty of the hand-assembled coils and sensors.

Even with a slightly non-ideal coil geometry, the field amplitude outside of the coils is less than 0.5% of the field amplitude at coil center. This is more than an order of magnitude improvement over a Helmholtz coil and comparable to the cross-talk achieved in SQUIDs (Ruffieux *et al* 2017). Senor orientation is affected by a maximum of 0.5°. Due to the multiple windings of the new coil, the opposing fields generated by the inner and outer loops create a total field at the center, which is 1.33 times larger than that of the single-loop Helmholtz coil driving the same current. This was verified with a fluxgate magnetometer which fit inside the coil geometry.

We also measured the axial field component along the axial direction of the sensor in figure 5. This is important when considering gradiometry that uses two OPMs separated along the sensor axis. Our current MEG setup with a 2 cm baseline shows a 4% cross-talk between magnetometers with simple Helmholtz coils. With our new coil geometry, the cross-talk at 2 cm is reduced to 0.5%.

3.2. Field homogeneity

Large field inhomogeneity over the vapor cell broadens the atomic resonance line and reduces sensor dynamic range and sensitivity. The axial and radial profiles of the field around the vapor cell (figure 6) created by the new coil and a Helmholtz coil show that the new coil set largely preserves homogeneity. In the radial direction, the non-ideal (ideal) field remains 98.01% (98.86%) homogeneous over the 3 mm cell width (Helmholtz: 99.84%),

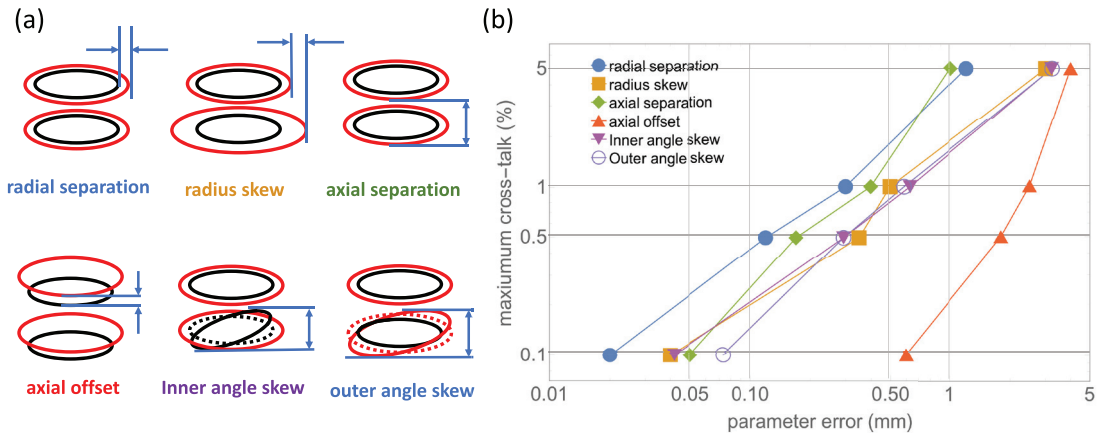

Figure 7. Theoretical estimate of cross-talk sensitivity to errors in four coil parameters. Radial separation: radial distance between inner and outer coils, radius skew: the difference in radius of front/back coils in either inner or outer coil set, axial separation: axial distance between front/back coils in either inner or outer coil set, axial offset: axial offset of inner and outer coils from one another, inner angle skew: axial distance due to inner coil tilt, and outer angle skew: axial distance due to outer coil tilt.

while in the axial direction the non-ideal (ideal) field shows 94.45% (99.09%) homogeneous over the 3 mm cell length (Helmholtz: 99.62%).

3.3. Reproducibility

To estimate our ability to experimentally reproduce the cross-talk result, we introduce errors into our theoretical model in several different coil parameters. We keep all errors zero and vary one parameter at a time to estimate how sensitive the cross-talk is to each parameter (figure 7(b)). The axial separation of the inner coils has an almost identical impact on error as the axial separation of the outer coils, so the two error sources have been combined to simplify the analysis. The separation in radius of the inner and outer coil is the most sensitive parameter with an absolute error allowance of 0.02 mm to achieve a maximum cross-talk of 0.1%. With more precise coil and sensor-assembly tools such as printed Kapton coils and 3D-printed sleeves, this specification is achievable.

4. Conclusion

A new double-coil geometry for zero-field OPM modulation and negative feedback was designed and built that reduces cross-talk between adjacent sensors to a maximum of 0.5% of the field at coil center. Cross-talk is more than a factor of 10 lower than that of a Helmholtz coil and less than 5% in field homogeneity is sacrificed over the volume of the vapor cell. Operating in closed-loop mode, sensors using the new coil geometry are sensitive to about 0.5% of the signal seen by an adjacent sensor. This enables an increased density of OPMs in future MEG arrays which will provide higher spatial resolution. The new design also exhibits lower cross-talk in the axial direction that is important for future tangential MEG arrays. With more precise alignment of coils, a cross-talk of less than 0.05% is possible in future designs.

Acknowledgments

This work has been supported by funds from the National Institutes of Health under grant numbers R01EB019440 and R01NS094604. The content is solely the responsibility of the authors and does not necessarily represent the official views of the National Institutes of Health.

ORCID iDs

N V Nardelli https://orcid.org/0000-0002-1558-5182

References

Allred J C, Lyman R N, Kornack T W and Romalis M V 2002 High-sensitivity atomic magnetometer unaffected by spin-exchange relaxation *Phys. Rev. Lett.* **89** 130801

Boto E, Bowtell R, Krüger P, Fromhold T M, Morris P G, Meyer S S, Barnes G R and Brookes M J 2016 On the potential of a new generation of magnetometers for MEG: a beamformer simulation study *PLoS One* **11** e0157655

Boto E *et al* 2018 Moving magnetoencephalography towards real-world applications with a wearable system *Nature* **555** 657–61
Dammers J, Chocholacs H, Eich E, Boers F, Faley M, Dunin-Borkowski R E and Shah N J 2014 Source localization of brain activity using helium-free interferometer *Appl. Phys. Lett.* **104** 213705
Dupont-Roc J, Haroche S and Tannoudji C 1969 Detection of very weak magnetic fields (10^{-9} gauss) by Rb zero-field level crossing resonances *Phys. Lett.* A **28** 628–39
Happer W and Tang H 1973 Spin-exchange shift and narrowing of magnetic resonance lines in optically pumped alkali vapors *Phys. Rev. Lett.* **31** 273–6
Iivanainen J, Stenroos M and Parkkonen L 2017 Measuring MEG closer to the brain: performance of on-scalp sensor arrays *NeuroImage* **147** 542–53
Jiménez-Martínez R, Knappe S and Kitching J 2014 An optically modulated zero-field atomic magnetometer with suppressed spin-exchange broadening *Rev. Sci. Instrum.* **85** 045124
Liew L A, Knappe S, Moreland J, Robinson H, Hollberg L and Kitching J 2004 Microfabricated alkali atom vapor cells *Appl. Phys. Lett.* **84** 2694–6
Luessi M, Nummenmaa A, Lew S, Okada Y and Hämäläinen M 2014 Performance evaluation of a novel pediatric MEG system *The 19th Int. Conf. of Biomagnetism (Halifax, Canada)*
Perry A R, Sheng D, Krzyzewski S P, Geller S and Knappe S 2017 Microfabricated optically-pumped magnetic arrays for biomedical imaging *Proc. SPIE* **10119** 101190V
Pfeiffer C, Ruffieux S, Jönsson L, Chukharkin M L, Kalaboukhov A, Xie M, Winkler D and Schneiderman J F 2019 A 7-channel high-Tc SQUID-based on-scalp MEG system *IEEE Trans. Biomed. Eng.* (https://doi.org/10.1109/TBME.2019.2938688)
Ruffieux S, Xie M, Chukharkin M, Pfeiffer C, Kalabukhov A, Winkler D and Schneiderman J F 2017 Feedback solutions for low crosstalk in dense arrays of high-Tc SQUIDs for on-scalp MEG *Supercond. Sci. Technol.* **30** 054006
Schwarz T, Wölbing R, Reiche C F, Müller B, Martínez-Pérez M J, Mühl T, Büchner B, Kleiner R and Koelle D 2015 Low-noise $YBa_2CU_3O_7$ nano-SQUIDs for performing magnetization-reversal measurements on magnetic nanoparticles *Phys. Rev. Appl.* **3** 044011
Sheng D, Perry A R, Krzyzewski S P, Geller S, Kitching J and Knappe S 2017 A microfabricated optically-pumped magnetic gradiometer *Appl. Phys. Lett.* **110** 031106
Simpson J C, Lane J E, Immer C D, Youngquist R C and Steinrock T 2001 Simple analytic expressions for the magnetic field of a circular current loop NASA Technical Document Collection (Washington, DC: NASA) (http://ntrs.nasa.gov/archive/nasa/casi.ntrs.nasa.gov/20010038494_2001057024.pdf)
Supek S and Aine C 2014 *Magnetoencephalography—From Signals to Dynamic Cortical Networks* (Springer: Berlin) p 1013
Taulu S 2008 Processing of weak magnetic multichannel signals: the signal space separation method *PhD Thesis* (Finland: Helsinki University of Technology)
ter Brake H J, Fleuren F H, Ulfman J A and Flokstra J 1986 Elimination of flux-transformer crosstalk in multichannel SQUID magnetometers *Cryogenics* **26** 667–70
Zhang Y, Tavrin Y, Mück M, Braginski A I, Heiden C, Hampson S, Pantev C and Elbert T 1993 Magnetoencephalography using high temperature rf SQUIDs *Brain Topol.* **5** 379–82